Wave diffraction from a truncated cylinder with a moonpool of arbitrary cross-section: a semi-analytical study

Zheng, Siming
State Key Laboratory of Coastal and Offshore Engineering, Dalian University of Technology

Gao, Wei
Research Institute for Applied Mechanics, Kyushu University

Liu, Yingyi
Research Institute for Applied Mechanics, Kyushu University

Cheng, Shanshan
School of Engineering, Computing and Mathematics, University of Plymouth

出版情報：Ocean Engineering. 237 (109573), 2021-10-01. Elsevier
バージョン：
権利関係：

Wave diffraction from a truncated cylinder with a moonpool of arbitrary cross-section: a semi-analytical study

Siming Zheng[a,b], Wei Gao[c], Yingyi Liu[d,*], Shanshan Cheng[b]

[a]*State Key Laboratory of Coastal and Offshore Engineering, Dalian University of Technology, Dalian, 116024, China*
[b]*School of Engineering, Computing and Mathematics, University of Plymouth, Drake Circus, Plymouth PL4 8AA, UK*
[c]*CNOOC Research Institute Ltd., Beijing 100028,China*
[d]*Research Institute for Applied Mechanics, Kyushu University, Fukuoka 8168580, Japan*

Abstract

In this paper, a semi-analytical model is proposed to solve the diffraction problem from a cylinder with a moonpool. The cylinder and the moonpool can be in arbitrary shapes. Linear potential flow theory and eigenfunction matching method are adopted in the analytical model. After dividing the fluid domain into three regions (i.e., the region beneath the cylinder; the inner region enclosed by the cylinder; the exterior region outer the cylinder), diffracted spatial potentials in each region can be expressed by a series of eigenfunctions. The continuity conditions between adjacent regions together with a Fourier series method combined with the eigenfunction matching method are employed to determine the unknown coefficients in the expressions of diffracted potentials. The well-known potential of incident waves and the obtained diffracted potentials are then used to directly compute the wave excitation forces/moments acting on the cylinder and the wave excitation volume flux. Analytical results of wave excitation forces/moments and volume flux are compared with the numerical results obtained by using a boundary element method numerical solver. Wave diffraction from the cases with different shapes of either cylinder hull or moonpool is finally tested with the semi-analytical model.

*Corresponding author. Email: liuyingyi@riam.kyushu-u.ac.jp

Keywords: Wave structure interaction, Potential flow theory, Semi-analytical model, Wave excitation forces/moments, Eigenfunction matching method

1. Introduction

In drillships, construction vessels, some offshore floating platforms and offshore wave energy converters, there are vertical openings from deck to keel through the hulls, which are the features known as 'moonpools' (see Fig. 1). It has been proved that the existence of the moonpool could strongly influence the hydrodynamic forces and motion response of these offshore structures (Molin, 2001; Wei et al., 2011; Guo et al., 2017; Molin et al., 2018; Miquel et al., 2020).

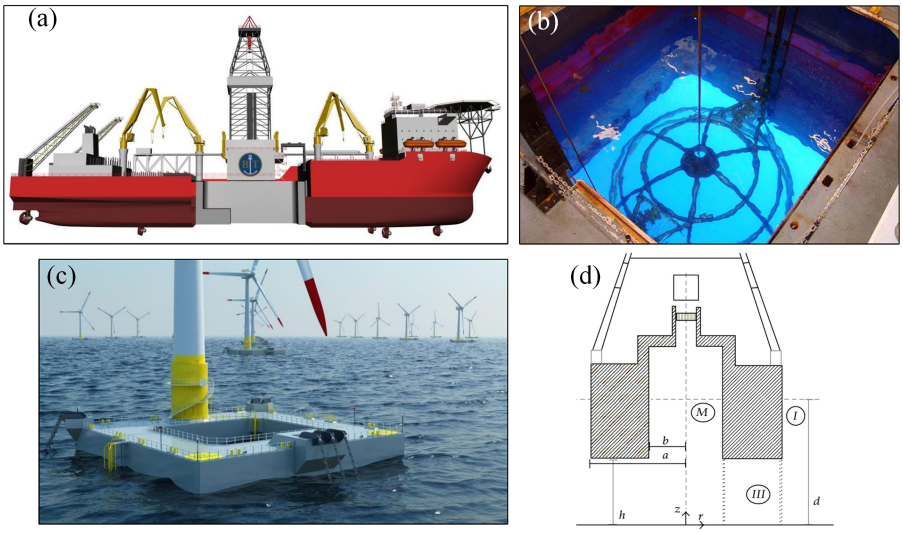

Figure 1: Moonpools in offshore structures: (a) drill ship (Hammargren and Törnblom, 2012); (b) dedicated ROV (Remotely Operated Underwater Vehicle) moonpool in a vessel (Laughlin, 2010); (c) floating platform used in offshore wind power (Dodd, 2015); (d) oscillating water column (OWC) (Mavrakos and Konispoliatis, 2012)

To explore the exact interaction between the offshore structure consisting of a moonpool and gravity waves, many analytical models have been developed since 1970s. In 1970, Garrett (1970) presented an analytical model to consider the excitation of waves inside a bottomless harbor, in which the harbor was

represented by a partially immersed hollow circular cylinder with the walls infinitely thin, enclosing a moonpool that takes over the entire cylinder. The diffracted waves in the moonpool and outside the cylinder were both expanded in Bessel functions and modified Bessel functions. A least-squares minimization method was then employed to determine the unknown coefficients in the expressions of diffracted potentials. Following Garrett (1970), the diffraction problem from a hollow cylindrical shell structure was investigated by Zhu and Mitchell (2009), whereas a different and more direct method was employed to solve the diffracted potentials. In preliminary design and parametric studies of offshore structures, estimating the wave loads is required. Analytical solutions of the exciting sway force and pitch moment acting on the hollow cylindrical shell structure, together with hydrodynamic coefficients, were given by Miloh (1983), and they were found to compare favorably with some experimental results. Since the wall was assumed to be infinitely thin, the exciting heave force was not calculated. Later, such assumption was released by Mavrakos (1985), who considered a circular cylinder with a circular moonpool with finite wall-thickness, i.e., a ring-shaped structure. The excitation forces in translation and rotation modes acting on the cylinder were all obtained by solving the wave diffraction problem through the employment of the Galerkin method. The results showed that, for long waves, the vertical force on the cylinder increased with the increase of wall thickness. As an extension to this work, Mavrakos (1988) adopted a similar analytical approach for evaluating the hydrodynamic parameters, i.e., added mass and damping coefficients, of the same case. Additionally, the diffraction and radiation problems from a thick-walled cylindrical body consisting of a moonpool with the bottom of cylinder partially open were analytically investigated by Zhou and Zhang (2013). The prediction of wave motion inside the moonpool based on the potential theory is generally exaggerated at the resonance frequencies due to a lack of viscous dissipation. This deviation can be eliminated by introducing the dissipation in some specified fluid domain, e.g., adding an additional term associated with the fluid viscosity in the boundary conditions at the free surface of the moonpool (Chen et al.,

2015); introducing an extra virtual dissipative disc at the moonpool entrance (Liu et al., 2017).

As waves approach an oscillating water column (OWC) device, the water column enclosed by the chamber, i.e., the moonpool, will be excited to oscillate, driving the air inside the chamber flowing through the turbine and hence generating electricity. Hence the excitation volume flux of the moonpool is of great significance for evaluating the performance of the OWC device. Evans and Porter (1997) presented a theoretical model for solving both wave diffraction and radiation of a thin-walled OWC and obtained the maximum absorbed power when the volume flow rate across through the turbine can be optimized. An OWC device with finite wall thickness was examined by Mavrakos and Konispoliatis (2012) employing an analytical method based on matched axisymmetric eigenfunction expansions of the velocity potential. Completed hydrodynamic analysis, including the evaluation of the first-order wave excitation forces, the airflow flux, the hydrodynamic parameters, and the maximum absorbed power, can be achieved with their analytical model. More recently, the analytical model for individual offshore OWC was extended to the hydrodynamic analysis of a coast/breakwater integrated OWC and an array of OWCs along a straight coast (e.g. see Zheng et al., 2019a,b).

All these aforementioned research work are about a circular-shaped cylinder with a circular moonpool. In practice, the moonpool or/and the offshore structure could be non-circular, e.g., the floating platform as shown in Fig. 1c is a square cylinder with a square moonpool. To evaluate the free-surface response inside a square moonpool, Molin (2001) derived simple quasi-analytical approximations based on the assumption of infinite water depth and infinite length and beam of the offshore structures that contain the moonpools. More recently, Molin et al. (2018) extended the theoretical model of Molin (2001) and proposed a different approach which applied to the finite water depth and the offshore structure with limited horizontal dimensions. Simple formulae were also derived based on so-called single-mode approximations to give the resonant frequencies. However, in their model, the velocity potential at a fictitious outer cylinder was

taken to be nil, which is a somewhat gross condition to ensure the connection with the exterior domain.

An obvious drawback of these analytical models as reviewed above is that they can only be applied to an offshore structure with a moonpool in circular cross-section, or be approximately implemented for that with a rectangular moonpool neglecting velocity potential in an exterior domain.

In this article, we consider a cylinder with a moonpool, in which both of them can be in arbitrary shapes. A semi-analytical model based on usual assumptions of linearized wave-body interactions is proposed to solve the wave diffraction problem. The fluid domain is divided into three regions: (a) the region beneath the cylinder; (b) the inner region enclosed by the cylinder, i.e., the moonpool; (c) the exterior region outside the cylinder. Diffracted spatial potentials in each region can be expressed by a series of eigenfunctions. A Fourier series method combined with the eigenfunction matching method is applied to satisfy the continuity conditions between adjacent regions and to determine the unknown coefficients in the expression of diffracted potentials. Wave excitation forces/moments and wave excitation volume flux are then evaluated by using the incident and diffracted wave potentials. The semi-analytical model is then employed to run a series of case studies.

The remainder of this paper is organized as follows. §2 presents a mathematical model for solving wave diffraction from a truncated cylinder with a moonpool of an arbitrary cross-section. A comparison of the analytical results of a cosine shaped hollow cylinder with the numerical ones by using three different numerical solvers can be found in §3. Moreover, the case studies on wave diffraction problem of a platform with different shapes of cross-section and a square platform with different dimensions are carried out with the employment of the semi-analytical model, the results and discussions of which are given in §3. Finally, conclusions are drawn in §4.

2. Mathematical model

Figure 2 gives a definition sketch of a truncated cylinder with a moonpool of an arbitrary cross-section. Both the Cartesian coordinate system ($Oxyz$) and the cylindrical coordinate system ($Or\theta z$) are adopted, in which a point at the center of the moonpool locating on mean water level is used as their origin O. The plane of $z = 0$ (i.e., the plane of Oxy) coincides with the still-water level with the positive Oz axis pointing upwards. The cylinder is subjected to a train of regular waves propagating in the direction of β relative to the position Ox axis with an angular frequency ω and a small amplitude A. The immersion depth of the cylinder and the water depth are denoted as d and h, respectively. $r_{in}(\theta)$ and $r_{out}(\theta)$ are the radius functions of the moonpool surface and the cylinder outer surface, respectively.

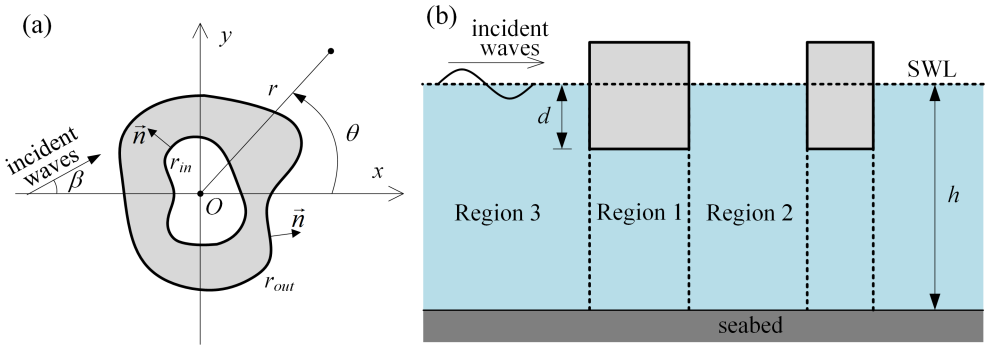

Figure 2: Definition sketch: (a) plan view; (b). side view

The unit normals on vertical surfaces of the cylinder with a moonpool directed towards far-field can be written as

$$\begin{aligned}\vec{n} &= \frac{1}{\sqrt{1+\left(\frac{1}{r}\frac{\partial S}{\partial \theta}\right)}}\left(\vec{e}_r + \frac{1}{r}\frac{\partial S}{\partial \theta}\vec{e}_\theta + 0\vec{e}_z\right) \\ &= \frac{1}{\sqrt{1+\left(\frac{1}{r}\frac{\partial S}{\partial \theta}\right)}}\left[\left(\cos\theta - \frac{1}{r}\frac{\partial S}{\partial \theta}\sin\theta\right)\vec{i} + \left(\sin\theta + \frac{1}{r}\frac{\partial S}{\partial \theta}\cos\theta\right)\vec{j} + 0\vec{k}\right],\end{aligned} \tag{1}$$

where$(\vec{e}_r, \vec{e}_\theta, \vec{e}_z)$ and $(\vec{i}, \vec{j}, \vec{k})$ are the unit basis vectors in the $Or\theta z$ and $Oxyz$

systems, respectively; S represents S_{out} and S_{in}, which are expressed as

$$S_{out} = r - r_{out}(\theta), \tag{2}$$

and

$$S_{in} = r - r_{in}(\theta), \tag{3}$$

respectively.

For small wave conditions, the usual inviscid incompressible linearized water wave theory may be in operation and a time factor of $\mathrm{e}^{-\mathrm{i}\omega t}$ is suppressed so that the fluid motion can be described by the velocity potential $\Phi = \Re[\phi(x, y, z)\mathrm{e}^{-\mathrm{i}\omega t}]$, where ϕ can be further decomposed as $\phi = \phi_I + \phi_D$, in which

$$\phi_I = -\frac{\mathrm{i}gA}{\omega}\frac{\cosh[k_0(z+h)]}{\cosh(k_0 h)}\sum_{m=-\infty}^{\infty}\mathrm{i}^m\mathrm{e}^{-\mathrm{i}m\beta}J_m(k_0 r)\mathrm{e}^{\mathrm{i}m\theta}, \tag{4}$$

is the undisturbed incident wave potential with J_m the Bessel function of the mth order, g the gravity acceleration, k_0 the wave number satisfying $\omega^2 = gk_0\tanh(k_0 h)$, and ϕ_D is a solution of the governing equations

$$\frac{\partial^2\phi_D}{\partial x^2} + \frac{\partial^2\phi_D}{\partial y^2} + \frac{\partial^2\phi_D}{\partial z^2} = 0, \text{ in the fluid} \tag{5}$$

with

$$\frac{\partial\phi_D}{\partial z} - \frac{\omega^2}{g}\phi_D = 0, \text{ on } z = 0 \text{ and } r > r_{out}, r < r_{in}, \tag{6}$$

$$\frac{\partial\phi_D}{\partial z} = 0, \text{ on } z = -h, \tag{7}$$

$$\frac{\partial\phi_D}{\partial z} = -\frac{\partial\phi_I}{\partial z}, \text{ on } z = -d \text{ and } r_{in} < r < r_{out}, \tag{8}$$

$$\frac{\partial\phi_D}{\partial n} = -\frac{\partial\phi_I}{\partial n}, \text{ on } -d < z < 0 \text{ and } r = r_{out},\ r = r_{in}, \tag{9}$$

and

$$\sqrt{k_0 r}\left(\frac{\partial\phi_D}{\partial r} - \mathrm{i}k_0\phi_D\right) = 0, \text{ on } r \to \infty. \tag{10}$$

2.1. Expressions of the diffracted velocity potentials

As shown in Fig. 2b, the fluid domain is divided into three regions, (a) Region 1, i.e., the domain beneath the cylinder; (b) Region 2, i.e., the moonpool region; and (c) Region 3, i.e., the remainder extending towards infinite distance horizontally.

The diffracted velocity potential in Region 1 (i.e., the domain beneath the cylinder), $\phi_{D,1}$, may be expressed as

$$\phi_{D,1}(r,\theta,z) = -\phi_I + \sum_{m=-\infty}^{\infty}\left[E_{m,0} + \sum_{l=1}^{\infty}\left(A_{m,l}I_m(\beta_l r) + B_{m,l}K_m(\beta_l r)\right)\cos[\beta_l(z+h)]\right]\mathrm{e}^{\mathrm{i}m\theta}, \tag{11}$$

where

$$\beta_l = \frac{l\pi}{h-d},\ l = 0,1,2,\cdots, \tag{12}$$

$$E_{m,0} = \begin{cases} A_{m,0} + B_{m,0}\ln(r), & m = 0 \\ A_{m,0}r^{|m|} + B_{m,0}r^{-|m|}, & m \neq 0 \end{cases}, \tag{13}$$

$A_{m,l}$ and $B_{m,l}$ are the unknown coefficients to be determined, I_m and K_m represent the modified Bessel functions of the first kind and the second kind, respectively, of the mth order.

An approximate expression of the diffracted velocity potential in Region 2 (i.e., the moonpool region), $\phi_{D,2}$, may be written as

$$\phi_{D,2}(r,\theta,z) = \sum_{m=-\infty}^{\infty}\left[C_{m,0}J_m(k_0 r)\frac{Z_0(z)}{Z_0(0)} + \sum_{l=1}^{\infty}C_{m,l}I_m(k_l r)\frac{Z_l(z)}{Z_l(0)}\right]\mathrm{e}^{\mathrm{i}m\theta}, \tag{14}$$

where $Z_0(z) = N_0^{-1/2}\cosh[k_0(z+h)]$, and $Z_l(z) = N_l^{-1/2}\cos[k_l(z+h)]$, in which $N_0 = \frac{1}{2}\left[1 + \frac{\sinh(2k_0h)}{2k_0h}\right]$ and $N_l = \frac{1}{2}\left[1 + \frac{\sin(2k_lh)}{2k_lh}\right]$; k_l for $l = 1,2,3,\cdots$ are the roots of

$$\omega^2 = -k_l g\tan(k_l h),\ l = 1,2,3,\cdots; \tag{15}$$

and $C_{m,l}$ are the unknown coefficients to be determined.

The diffracted velocity potential in Region 3 (i.e., the region extending towards infinite distance horizontally), $\phi_{D,3}$, may be expressed as

$$\phi_{D,3}(r,\theta,z) = \sum_{m=-\infty}^{\infty}\left[D_{m,0}H_m(k_0 r)\frac{Z_0(z)}{Z_0(0)} + \sum_{l=1}^{\infty} D_{m,l}K_m(k_l r)\frac{Z_l(z)}{Z_l(0)}\right]\mathrm{e}^{\mathrm{i}m\theta}, \tag{16}$$

approximately, where H_m is the Hankel function of the first kind of the mth order and $D_{m,l}$ are the unknown coefficients to be determined.

2.2. Solution of the unknown coefficients

The velocity potentials as given in Eqs. (11), (14) and (16) satisfy the governing equation and boundary conditions as listed in Eqs. (5)-(8) and (10). Eq. (9) and the continuity of pressure and the radial velocity at the interfaces between the adjacent regions can be merged into

$$\phi_{D,2}\big|_{S_{in}=0} = \phi_{D,1}\big|_{S_{in}=0},\ -h < z < -d, \tag{17}$$

$$\phi_{D,3}\big|_{S_{out}=0} = \phi_{D,1}\big|_{S_{out}=0},\ -h < z < -d, \tag{18}$$

$$\left(r^2(\theta)\frac{\partial\phi_{D,2}}{\partial r} + \frac{\partial S_{in}}{\partial\theta}\frac{\partial\phi_{D,2}}{\partial\theta}\right)\Big|_{S_{in}=0} = \begin{cases} -\left(r^2(\theta)\frac{\partial\phi_I}{\partial r} + \frac{\partial S_{in}}{\partial\theta}\frac{\partial\phi_I}{\partial\theta}\right)\Big|_{S_{in}=0}, & -d < z < 0 \\ \left(r^2(\theta)\frac{\partial\phi_{D,1}}{\partial r} + \frac{\partial S_{in}}{\partial\theta}\frac{\partial\phi_{D,1}}{\partial\theta}\right)\Big|_{S_{in}=0}, & -h < z < -d \end{cases}, \tag{19}$$

$$\left(r^2(\theta)\frac{\partial\phi_{D,3}}{\partial r} + \frac{\partial S_{in}}{\partial\theta}\frac{\partial\phi_{D,3}}{\partial\theta}\right)\Big|_{S_{out}=0} = \begin{cases} -\left(r^2(\theta)\frac{\partial\phi_I}{\partial r} + \frac{\partial S_{in}}{\partial\theta}\frac{\partial\phi_I}{\partial\theta}\right)\Big|_{S_{out}=0}, & -d < z < 0 \\ \left(r^2(\theta)\frac{\partial\phi_{D,1}}{\partial r} + \frac{\partial S_{out}}{\partial\theta}\frac{\partial\phi_{D,1}}{\partial\theta}\right)\Big|_{S_{out}=0}, & -h < z < -d \end{cases}, \tag{20}$$

which should also be satisfied and employed to determine the unknown coefficients $A_{m,l}$, $B_{m,l}$, $C_{m,l}$ and $D_{m,l}$. Details are given in Appendix A.

2.3. Expressions of the wave excitation forces/moments and volume flux

Once the wave diffracted velocity is known, the hydrodynamic pressure in the flow domain can be estimated by the linearized Bernoulli equation, and the wave excitation forces/moments acting on the truncated cylinder can be further evaluated by integrating the hydrodynamic pressure over the wetted surface of the cylinder. These quantities are listed as follows:

(1) Wave excitation force in x direction $F_e^{(1)}$

$$F_e^{(1)} = -\mathrm{i}\omega\rho \int_0^{2\pi} \int_{-d}^{0} \left\{ \left[\left(r\cos\theta - \frac{\partial S_{out}}{\partial \theta}\sin\theta \right) (\phi_I + \phi_{D,3}) \right] \Big|_{S_{out}=0} - \left[\left(r\cos\theta - \frac{\partial S_{in}}{\partial \theta}\sin\theta \right) (\phi_I + \phi_{D,2}) \right] \Big|_{S_{in}=0} \right\} \mathrm{d}z\mathrm{d}\theta \tag{21}$$

(2) Wave excitation force in y direction $F_e^{(2)}$

$$F_e^{(2)} = -\mathrm{i}\omega\rho \int_0^{2\pi} \int_{-d}^{0} \left\{ \left[\left(r\sin\theta + \frac{\partial S_{out}}{\partial \theta}\cos\theta \right) (\phi_I + \phi_{D,3}) \right] \Big|_{S_{out}=0} - \left[\left(r\sin\theta + \frac{\partial S_{in}}{\partial \theta}\cos\theta \right) (\phi_I + \phi_{D,2}) \right] \Big|_{S_{in}=0} \right\} \mathrm{d}z\mathrm{d}\theta \tag{22}$$

(3) Wave excitation force in z direction $F_e^{(3)}$

$$F_e^{(3)} = \mathrm{i}\omega\rho \int_0^{2\pi} \int_{r_{in}}^{r_{out}} (\phi_I + \phi_{D,1}) \big|_{z=-d} r\mathrm{d}r\mathrm{d}\theta. \tag{23}$$

(4) Wave excitation moment about x axis at the rotation center, i.e., $(r, z) = (0, z_0)$, of the cylinder $F_e^{(4)}$

$$\begin{aligned} F_e^{(4)} = {} & \mathrm{i}\omega\rho \int_0^{2\pi} \int_{-d}^{0} \left[\left(r\sin\theta + \frac{\partial S_{out}}{\partial \theta}\cos\theta \right) (\phi_I + \phi_{D,3}) \right] \Big|_{S_{out}=0} (z - z_0)\mathrm{d}z\mathrm{d}\theta \\ & -\mathrm{i}\omega\rho \int_0^{2\pi} \int_{-d}^{0} \left[\left(r\sin\theta + \frac{\partial S_{in}}{\partial \theta}\cos\theta \right) (\phi_I + \phi_{D,2}) \right] \Big|_{S_{in}=0} (z - z_0)\mathrm{d}z\mathrm{d}\theta \\ & +\mathrm{i}\omega\rho \int_0^{2\pi} \int_{r_{in}}^{r_{out}} (\phi_I + \phi_{D,1}) \big|_{z=-d} r^2 \sin\theta \mathrm{d}r\mathrm{d}\theta \end{aligned} \tag{24}$$

(5) Wave excitation moment about y axis at the rotation center, i.e., $(r, z) = (0, z_0)$, of the cylinder $F_e^{(5)}$

$$\begin{aligned} F_e^{(5)} = &-\mathrm{i}\omega\rho \int_0^{2\pi} \int_{-d}^{0} \left[\left(r\cos\theta - \frac{\partial S_{out}}{\partial \theta} \sin\theta \right) (\phi_I + \phi_{D,3}) \right] \Big|_{S_{out}=0} (z - z_0) \mathrm{d}z\mathrm{d}\theta \\ &+\mathrm{i}\omega\rho \int_0^{2\pi} \int_{-d}^{0} \left[\left(r\cos\theta - \frac{\partial S_{in}}{\partial \theta} \sin\theta \right) (\phi_I + \phi_{D,2}) \right] \Big|_{S_{in}=0} (z - z_0) \mathrm{d}z\mathrm{d}\theta \\ &-\mathrm{i}\omega\rho \int_0^{2\pi} \int_{r_{in}}^{r_{out}} (\phi_I + \phi_{D,1}) \big|_{z=-d} r^2 \cos\theta \mathrm{d}r\mathrm{d}\theta. \end{aligned} \tag{25}$$

(6) Wave excitation moment about z axis at the rotation center, i.e., $(r, z) = (0, z_0)$, of the cylinder $F_e^{(6)}$

$$\begin{aligned} F_e^{(6)} = &-\mathrm{i}\omega\rho \int_0^{2\pi} \int_{-d}^{0} \left[\frac{r\partial S_{out}}{\partial \theta} (\phi_I + \phi_{D,3}) \right] \Big|_{S_{out}=0} \mathrm{d}z\mathrm{d}\theta \\ &+\mathrm{i}\omega\rho \int_0^{2\pi} \int_{-d}^{0} \left[\frac{r\partial S_{in}}{\partial \theta} (\phi_I + \phi_{D,2}) \right] \Big|_{S_{in}=0} \mathrm{d}z\mathrm{d}\theta \end{aligned} \tag{26}$$

(7) Wave excitation volume flux $F_e^{(0)}$, which is of interest for evaluating the performance of an OWC device (e.g., see Evans and Porter, 1995; Zheng et al., 2019a)

$$F_e^{(0)} = \int_0^{2\pi} \int_0^{r_{in}} \frac{\partial(\phi_I + \phi_{D,2})}{\partial z} \Big|_{z=0} r\mathrm{d}r\mathrm{d}\theta = \frac{\omega^2}{g} \int_0^{2\pi} \int_0^{r_{in}} (\phi_I + \phi_{D,2}) \big|_{z=0} r\mathrm{d}r\mathrm{d}\theta \tag{27}$$

3. Results and discussions

The wave excitation forces/moments and volume flux may be normalized as follows:

$$\bar{F}_j = \begin{cases} \frac{\omega |F_e^{(j)}|}{ghA}, & \text{for } j = 0 \\ \frac{|F_e^{(j)}|}{\rho g h^2 A}, & \text{for } j = 1, 2, 3 \\ \frac{|F_e^{(j)}|}{\rho g h^3 A}, & \text{for } j = 4, 5, 6 \end{cases} \tag{28}$$

$$\varphi_j = \arg F_e^{(j)}, \tag{29}$$

where $\bar{F}_j$ and φ_j denote the non-dimensional amplitude and phase, respectively.

3.1. Comparison of semi-analytical results with numerical results

Boundary Element Methods (BEM) solvers, e.g., the commercial solvers, WAMIT and ANSYS-AQWA, and the open-source solver, NEMOH and HAMS, have been widely used to solve the hydrodynamic problems of a large variety of marine structures (e.g., see Bozzi et al., 2013; Zheng and Zhang, 2017; Miquel et al., 2017; Liu, 2019). A comparison of the present semi-analytical results with the BEM-based numerical results provides a manner to validate the present model.

We take the truncated cylinder with a moonpool of cosine-function-shaped cross section (see Fig. 3),

$$\frac{r_{in}}{d} = 0.5 + 0.1\cos[3(\theta + \pi)], \tag{30}$$

$$\frac{r_{out}}{d} = 1 + 0.1\cos(3\theta), \tag{31}$$

with $h = 2$ m, $d/h = 0.5$ and $\beta = 30^\circ$ as an example to demonstrate the performance of the present semi-analytical model and make a comparison with the numerical results by WAMIT.

A convergence analysis was carried out before doing any case studies. The semi-analytical model was coded with Fortran and run in a laptop with Intel(R) Core(TM) i7-8550U CPU @ 1.80GHz 1.99 GHz, 8.00 GB RAM and a 64-bit operating system. Figures 4 and 5 illustrate the impact of the angular and vertical truncated cutoffs (i.e. in terms of M and L), respectively, on the wave excitation forces and moments. The corresponding CPU time required for solving wave diffraction problem per wave frequency are plotted in Fig. 6. As expected, the more truncated angular and vertical terms of the infinite series are, the more CPU time is required to solve the wave diffraction problem. Hereinafter, $M = 12$ and $L = 8$ are adopted to obtain converged results.

Figures 7, 8 and 9 present the comparison results of the translation and rotation modes of wave excitation forces acting on the cylinder and also the wave excitation volume flux of the moonpool. An excellent agreement of the

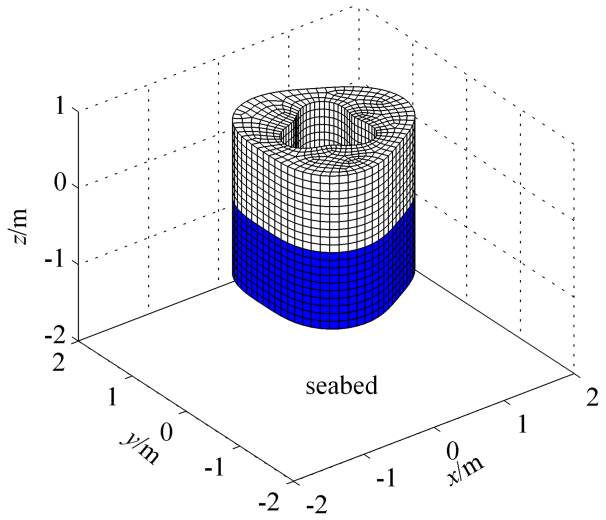

Figure 3: Computational mesh employed in the numerical solvers with the wetted surface marked in blue colour.

present analytical results with the numerical results of WAMIT is achieved in the computed range of wave frequencies. This gives confidence of the present semi-analytical model in solving water wave scattering problem of a truncated cylinder with a moonpool of arbitrary cross-section.

3.2. Case studies of an elliptic platform with different eccentricities

The validated model is applied to solve the wave diffraction problem of a platform with elliptic shapes (see Fig. 10).

The radius function of the platform outer surface is expressed as

$$r_{out}(\theta) = \frac{1}{\sqrt{\frac{\cos^2\theta}{a_1^2} + \frac{\sin^2\theta}{a_2^2}}}, \tag{32}$$

where a_1 and a_2 represent the width and height parameters, which are called the semi-major and semi-minor axes, respectively. The radius function of the moonpool surface is $r_{in}(\theta) = \frac{2}{3} r_{out}(\theta)$.

Figure 11 shows the wave excitation forces/moments acting on the elliptic platforms with different eccentricities for $\beta = 30°$, $d/h = 0.5$, $a_1 a_2 = d^2$, $a_2/a_1 = 0.5$, 0.8, 1.0, 1.25 and 2.0.

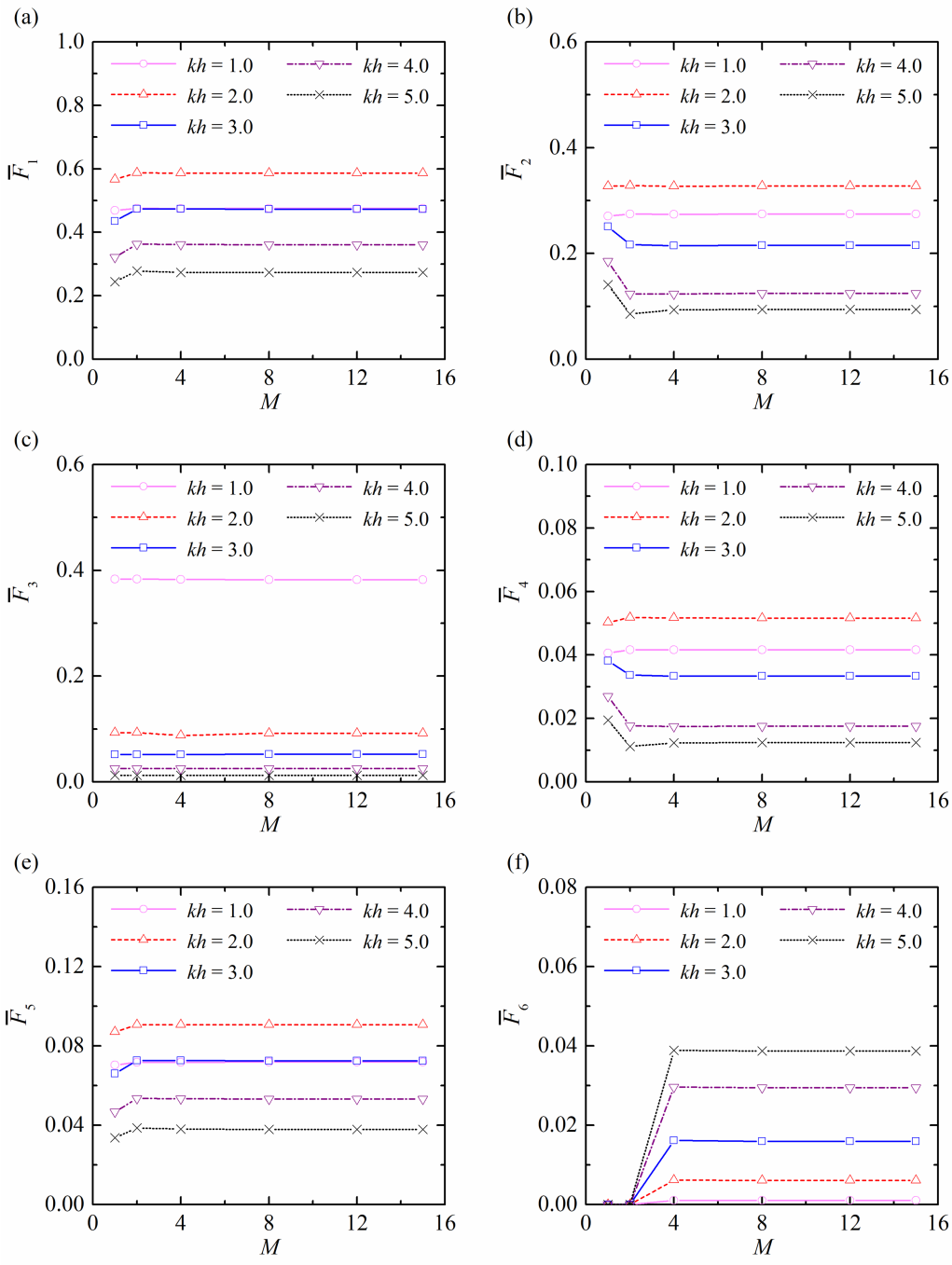

Figure 4: Impact of the angular cut-offs (i.e., in terms of M) on wave excitation forces/moments, $h = 2$ m, $d/h = 0.5$, $\beta = 30°$ and $L = 8$: (a) $\bar{F}_1$; (b) $\bar{F}_2$; (x) $\bar{F}_3$; (s) $\bar{F}_4$; (e) $\bar{F}_5$; (f) $\bar{F}_6$.

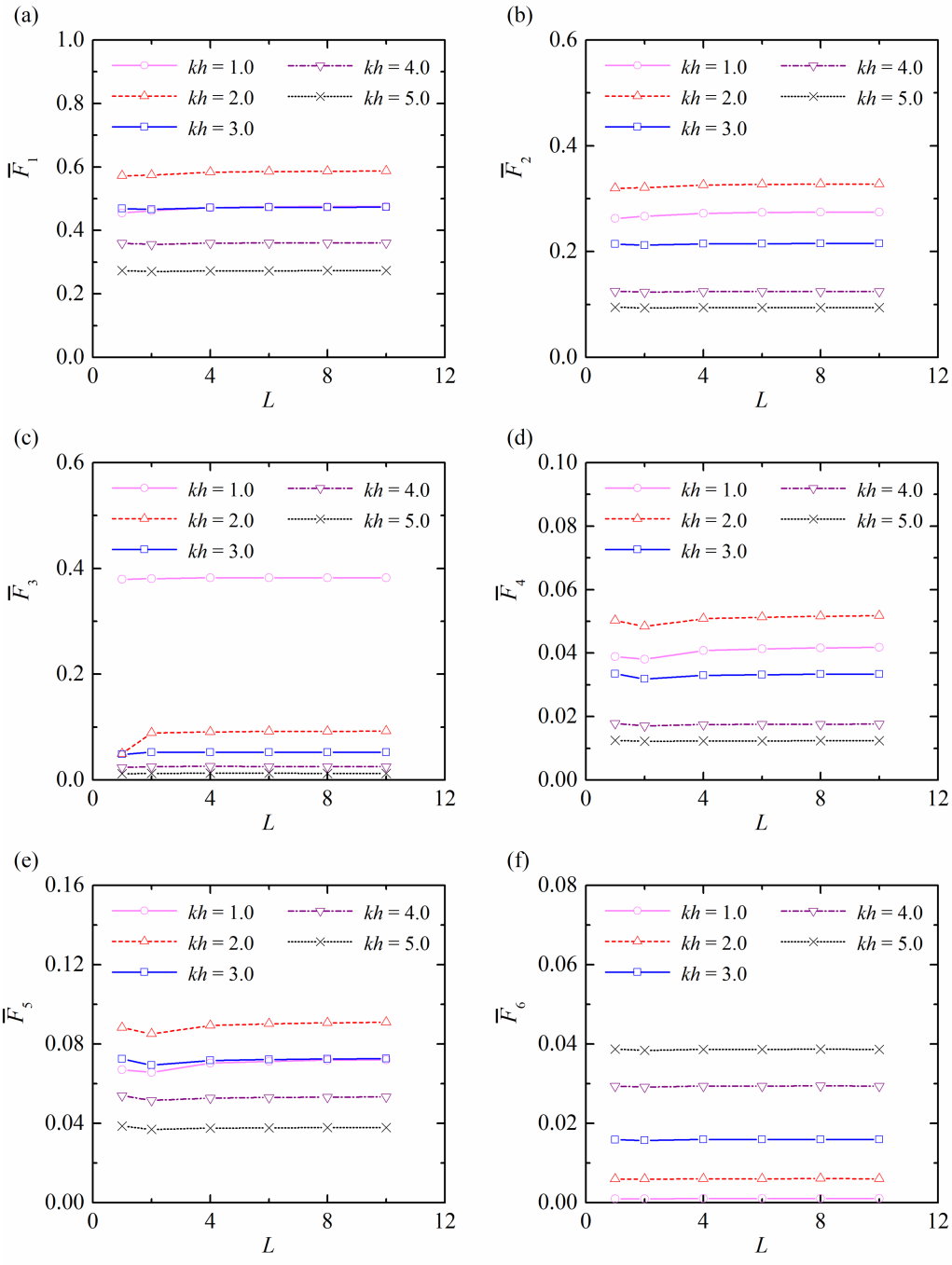

Figure 5: Impact of the vertical cut-offs (i.e., in terms of L) on wave excitation forces/moments, $h = 2$ m, $d/h = 0.5$, $\beta = 30°$ and $M = 12$: (a) $\bar{F}_1$; (b) $\bar{F}_2$; (x) $\bar{F}_3$; (s) $\bar{F}_4$; (e) $\bar{F}_5$; (f) $\bar{F}_6$.

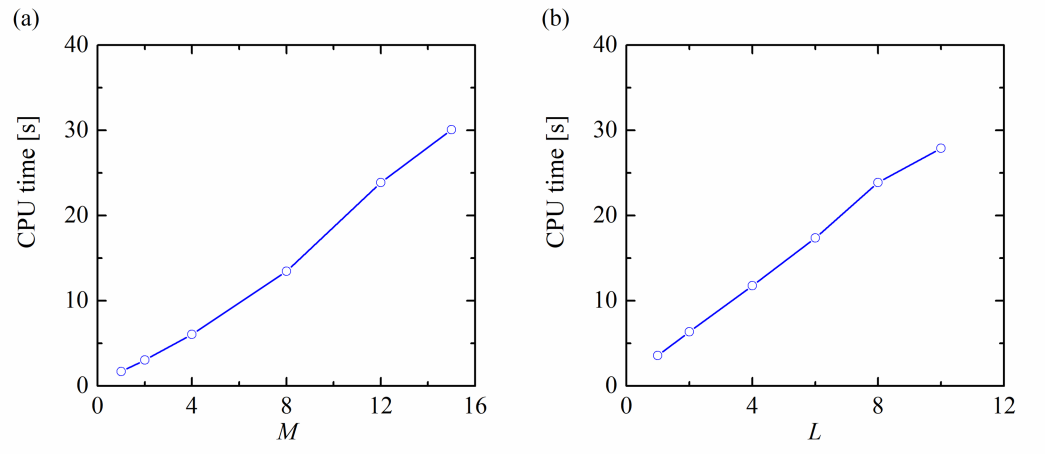

Figure 6: CPU time required per wave frequency: (a) variation with M for $L = 8$; (b) variation with L for $M = 12$.

In the computed range of wave conditions, $\bar{F}_1 - kh$ exhibits a single peak curve for $a_2/a_1 = 1.25$ and 2.0. Whereas for $a_2/a_1 = 0.5$, 0.8 and 1.0, apart from the main peak, sharp changes of the $\bar{F}_1 - kh$ curve are observed at $kh = 4.0$, 4.9 and 5.5, respectively. These sharp changes are excited due to the sloshing motion of water in the moonpool. As a_2/a_1 increases from 0.5 to 2.0, the main peak of the $\bar{F}_1 - kh$ curve rises. Similar contrasts are also seen in $\bar{F}_5 - kh$ (see Fig. 11e). For the $\bar{F}_2 - kh$ curves, sharp changes due to the sloshing motion of water in the moonpool are observed at the same wave conditions, i.e., $kh =$ 4.0, 4.9 and 5.5, as seen for the $\bar{F}_1 - kh$ curves. Nevertheless, those three sharp changes correspond to $a_2/a_1 = 2.0$, 1.25 and 1.0, respectively. The peak value of of $\bar{F}_2$ decreases with the increase of a_2/a_1. Similar variations are also seen in $\bar{F}_4 - kh$ (see Fig. 11d). The wave frequencies where the sharp changes of the $\bar{F}_3 - kh$ curves happen are found to be independent of the change of a_2/a_1. For the remaining computed wave conditions, the heave wave excitation force acting on the platform with $a_2/a_1 = 0.5$ is smaller than those for the other four examined cases with different values of a_2/a_1. As expected, $\bar{F}_6 = 0$ is obtained all over the computed range of wave conditions for a_2/a_1=1.0. For $kh < 2.0$, the yaw wave excitation moment acting on the platforms with a_2/a_1= 0.5 and

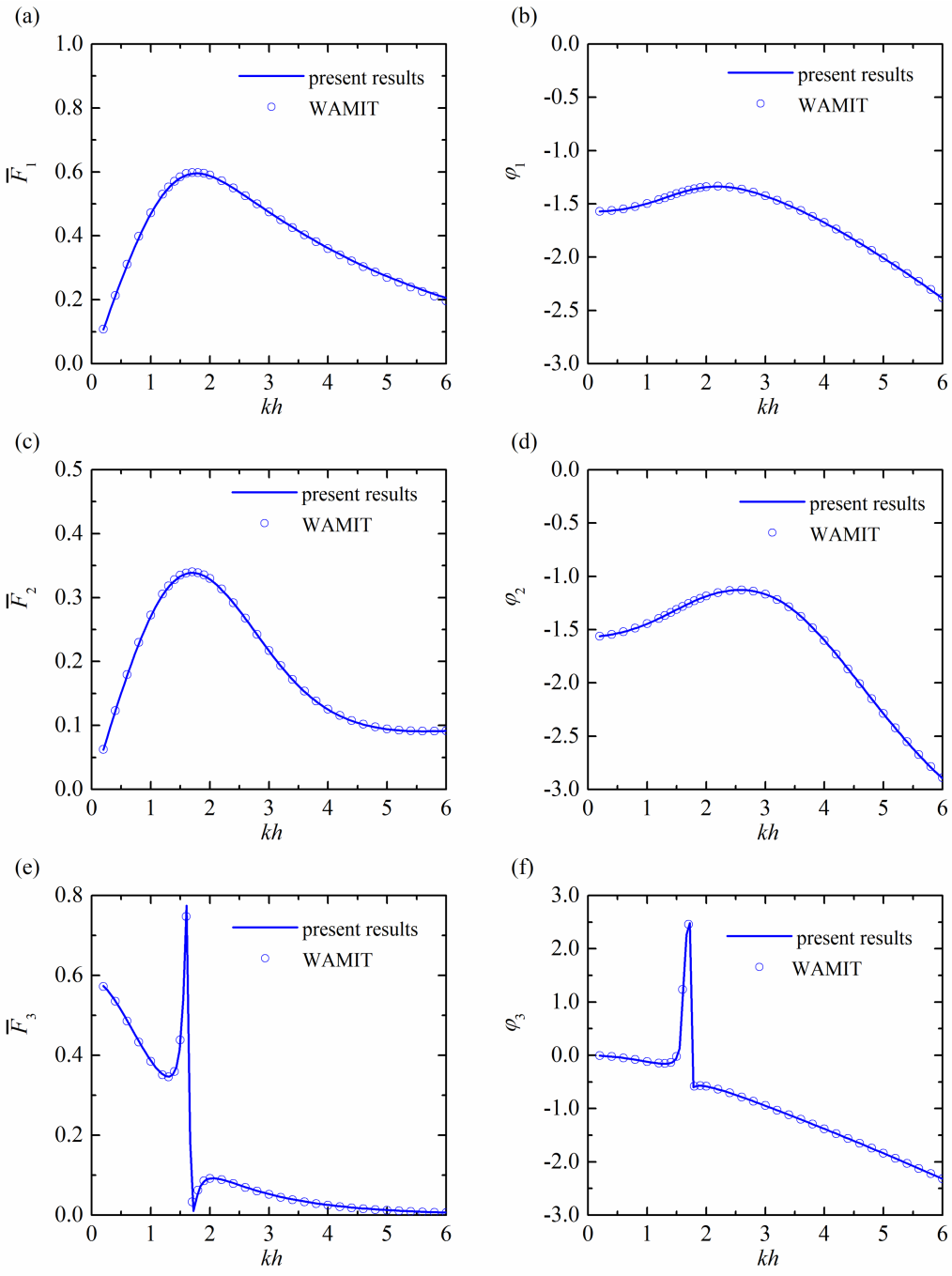

Figure 7: Comparison of present semi-analytical results with numerical results in terms of normalized excitation forces of the translation modes in the frequency domain as a function of kh with $h = 2$ m, $d/h = 0.5$ and $\beta = 30°$: (a) $\bar{F}_1$; (b) φ_1; (c) $\bar{F}_2$; (d) φ_2; (e) $\bar{F}_3$; (f) φ_3.

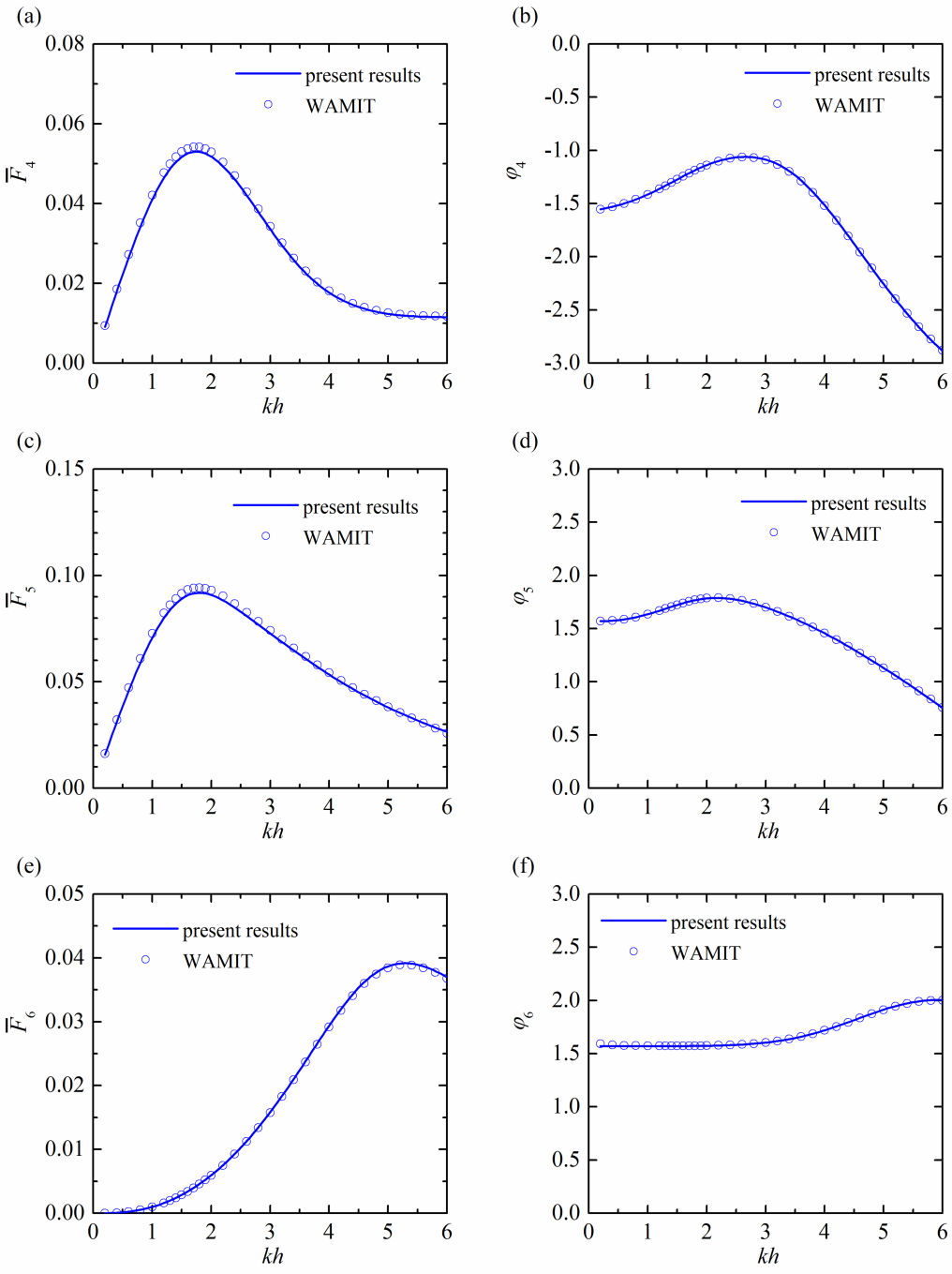

Figure 8: Comparison of present semi-analytical results with numerical results in terms of normalized excitation forces of the rotate modes in the frequency domain as a function of kh with $h = 2$ m, $d/h = 0.5$ and $\beta = 30°$: (a) $\bar{F}_4$; (b) φ_4; (c) $\bar{F}_5$; (d) φ_5; (e) $\bar{F}_6$; (f) φ_6.

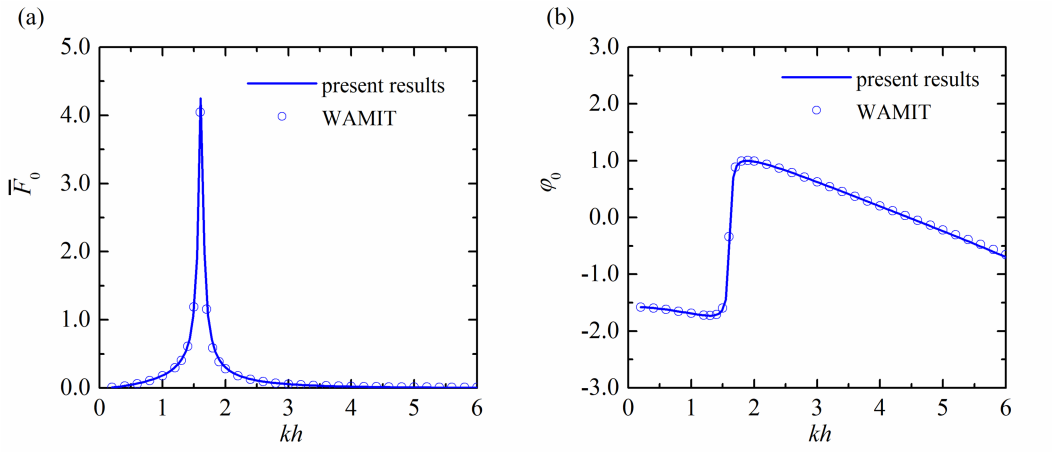

Figure 9: Comparison of present semi-analytical results with numerical results in terms of normalized excitation volume flux in the frequency domain as a function of kh with $h = 2$ m, $d/h = 0.5$ and $\beta = 30°$: (a) $\bar{F}_0$; (b) φ_0.

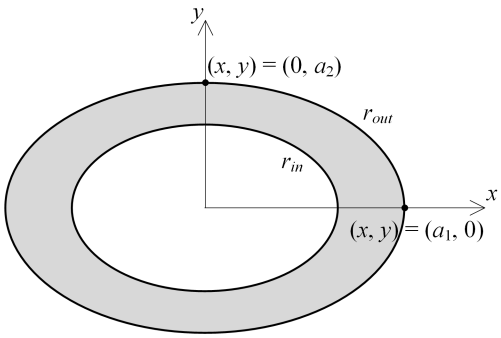

Figure 10: Schematic of the elliptic platform.

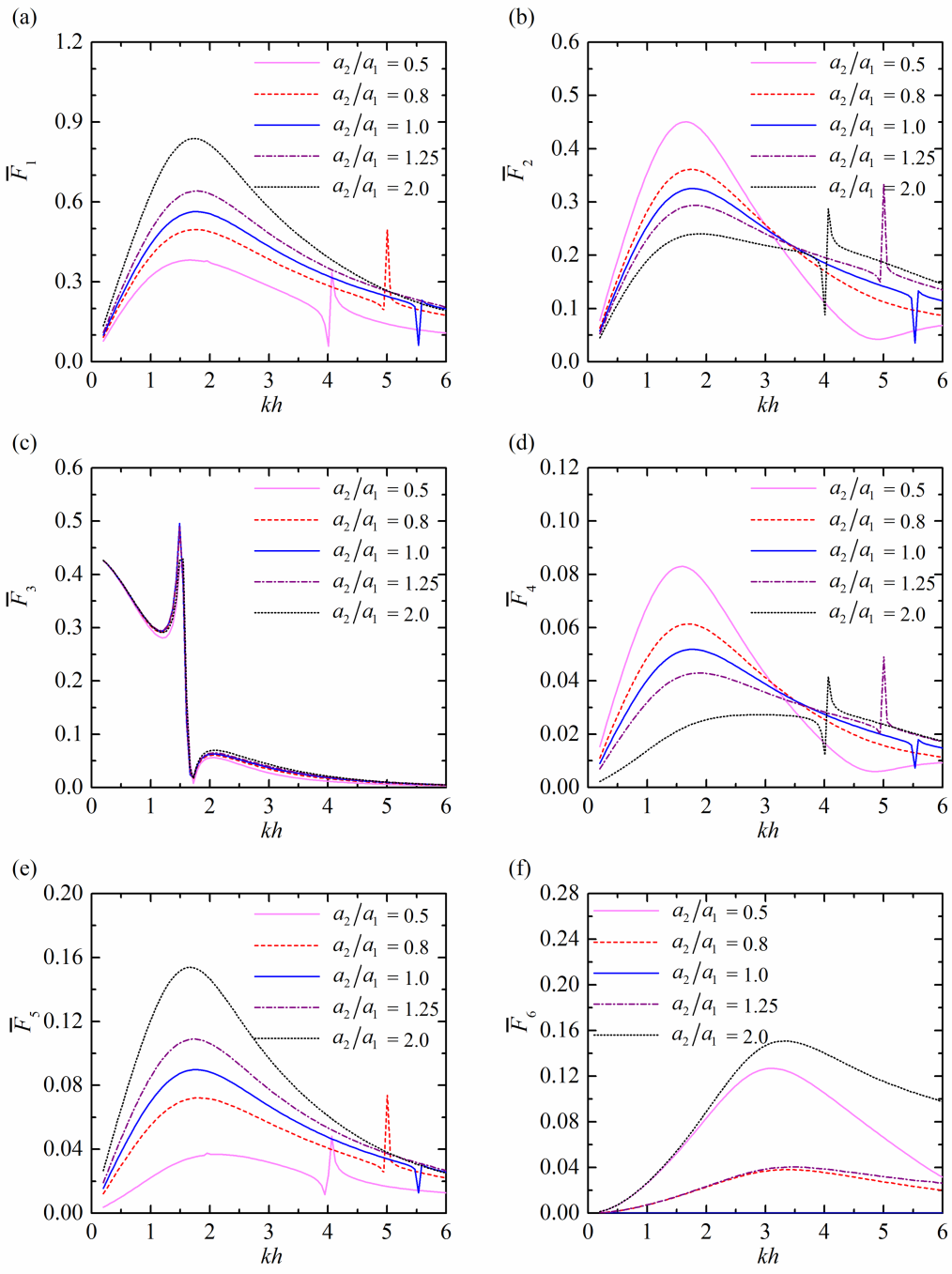

Figure 11: Effect of the elliptic eccentricities on wave excitation forces/moments: (a) $\bar{F}_1$; (b) $\bar{F}_2$; (c) $\bar{F}_3$; (d) $\bar{F}_4$; (e) $\bar{F}_5$; (f) $\bar{F}_6$ for $\beta = 30°$, $d/h = 0.5$, $a_1 a_2 = d^2$.

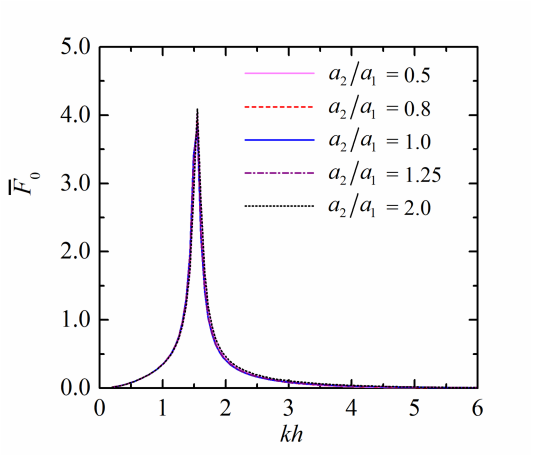

Figure 12: Effect of the elliptic eccentricities on wave excitation volume flux for $\beta = 30°$, $d/h = 0.5$, $a_1 a_2 = d^2$.

2.0 are almost the same. As kh increases from 2.0, the two $\bar{F}_6 - kh$ curves separate from one another. Similar contrasts are also seen in the two cases with a_2/a_1= 0.8 and 1.25. For $kh > 3.0$, the yaw wave excitation moment acting on the platform with $a_2/a_1 = 2.0$ is the largest among the five examined cases.

The results of the frequency response of the wave excitation volume flux are given in Fig. 12. The $\bar{F}_0 - kh$ curve is found to be insensitive to the change of a_2/a_1.

3.3. Case studies of a square platform with different outer hull widths

The semi-analytical model is also applied to a floating foundation for a wind turbine, which is a square float fitted with a square moonpool (see Fig. 1c). The foundation with a depth of 11 m floats at an offshore site of 55 m water depth, with 7 m immersed in the water. The widths of the outer hull and the moonpool are denoted as D_{out} and D_{in}, respectively. Assuming the mass is uniformly distributed all over the floating foundation, the center of gravity is 1.5 m below the mean water level, which is used as the reference point to evaluate the moments hereafter. The area of the square ring is assumed fixed (i.e., $D_{out}^2 - D_{in}^2 \equiv 1296\,\mathrm{m}^2$), therefore D_{in} will increase/decrease with the

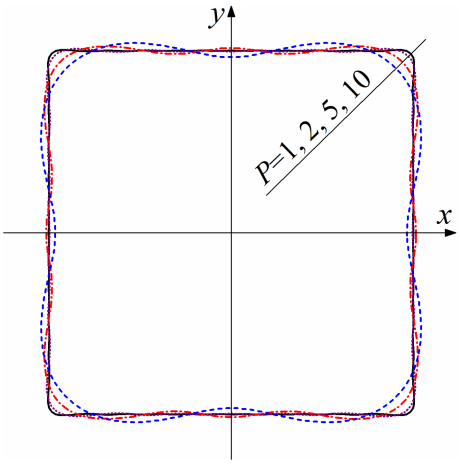

Figure 13: Approximation of the square by Eq. (33) with different terms retained, i.e., $p = 0, 1, 2, \cdots, P$ with $P = 1, 2, 5, 10$.

increase/decrease of D_{out}. Extremely, the moonpool disappears when the outer hull width $D_{out} = 36\,\mathrm{m}$.

To avoid singularity induced by a sharp edge, the square may be expanded into a series of Fourier terms in the present semi-analytical model. For a square with the width of D_{out}, the corresponding radius function can be expressed as

$$r_{out}(\theta) = \frac{D_{out}}{2} \sum_{p=0}^{\infty} R_p \cos(4p\theta), \tag{33}$$

where the values of R_p for $p = 0, 1, \cdots, 10$ are listed in Table 1.

Table 1: Values of R_p for $p = 0, 1, 2, \cdots, 10$

p	0	1	2	3	4	5	6	7	8	9	10
R_p	1.122	-0.157	0.049	-0.024	0.014	-0.009	0.006	-0.005	0.004	-0.003	0.002

The shapes given by the Eq. (33) with different truncated terms retained in the series (the terms with $p \leq P$ are kept) are plotted in Fig. 13. The approximation of the square cross-section with $P = 10$ is found to be reasonably good, and it is adopted hereinafter to represent the exact square cross-section.

Figure 14 presents frequency response of wave excitation forces/moments for different outer hull width in terms of D_{out}/h. For a solid platform (i.e., $D_{out}/h = 36/55$), there is no sharp change of the frequency response of any wave excitation component. As D_{out}/h increases, a square moonpool appears in the center of the platform and its dimension becomes larger and larger. Due to the existence of the moonpool, sharp changes of the frequency response of wave excitation forces/moments are observed and the larger the moonpool, the smaller kh where the main sharp change occurs. The main peaks of the rotation components of the excitation force as shown in Figs. 14d-14f become higher with the increase of D_{out}/h.

The wave excitation volume flux results as given in Fig. 15 demonstrate that as the dimension of the moonpool increases, the peak of the frequency response of $\bar{F}_0$ shifts towards low frequencies and meanwhile, both the bandwidth and peak height become larger. This result may be of interest to the design of a floating OWC device.

4. Discussions

It is well known that Eq. (16) is valid outside a circular cylinder encompassing the outer waterline, of radius $R_o = max\{r_{out}(\theta)\}$. For the remaining sub-regions of Region 3, i.e., $r_{out}(\theta) < r(\theta) < R_o$, strictly speaking, apart from the H_m and K_m associated terms as shown in Eq. (16), the J_m and I_m related terms should also be considered. Likewise Eq. (14) is valid inside a circular cylinder contained inside the moonpool, of radius $R_i = min\{r_{in}(\theta)\}$. In a similar way, strictly more complicated expressions are required for the remaining sub-regions of Region 1. However, this will make the semi-analytical model much more complicated due to more unknown coefficients to be solved and more continuity conditions at the interfaces between the sub-regions and the corresponding outside/inside circular-shaped region.

In this paper, for the sake of simplicity, Eqs. (16) and (14) are employed to approximately express the velocity potential all over Regions 3 and 1, re-

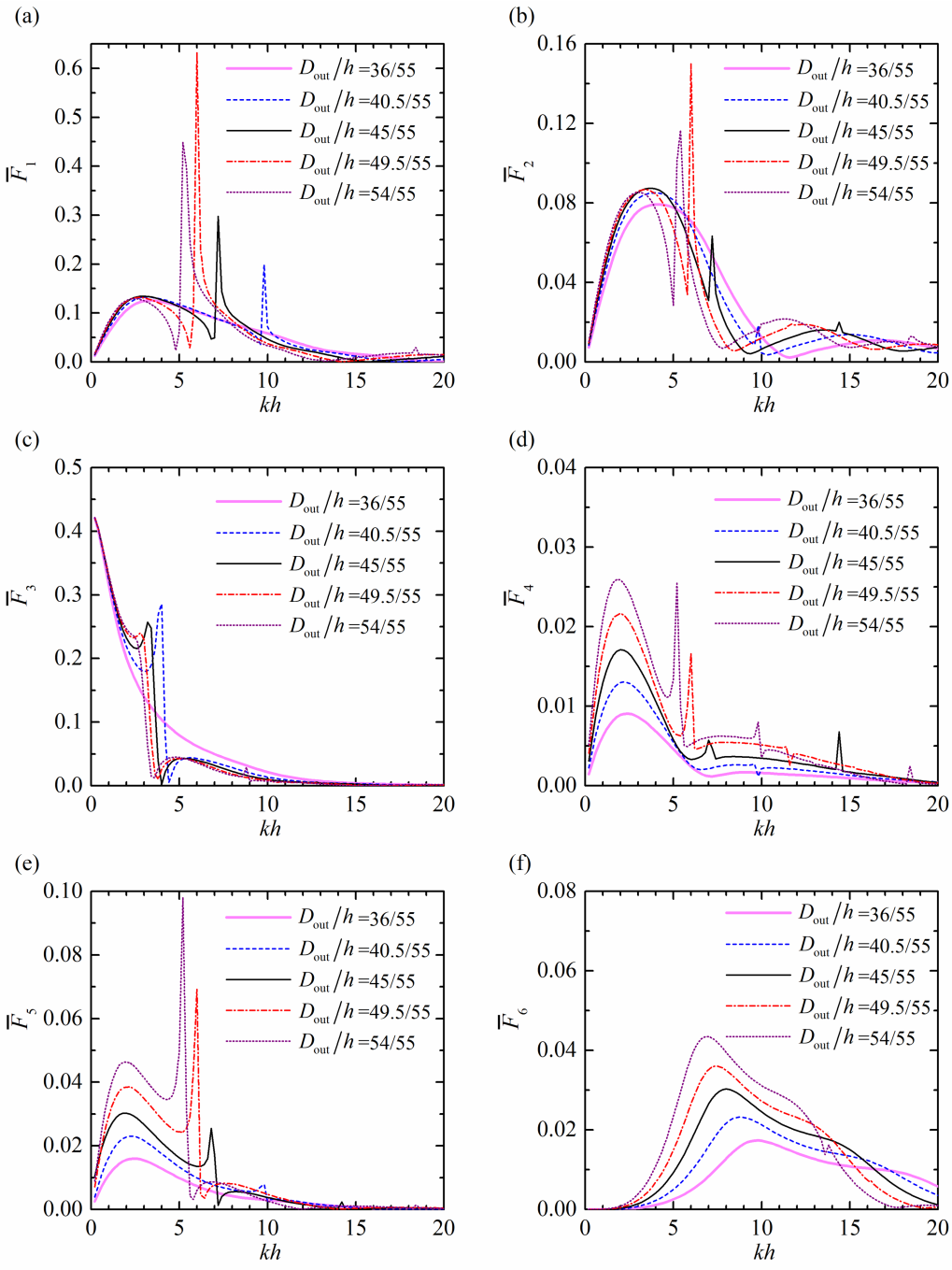

Figure 14: Effect of the outer hull width of a square hollow platform on wave excitation forces/moments: (a) $\bar{F}_1$; (b) $\bar{F}_2$; (c) $\bar{F}_3$; (d) $\bar{F}_4$; (e) $\bar{F}_5$; (f) $\bar{F}_6$.

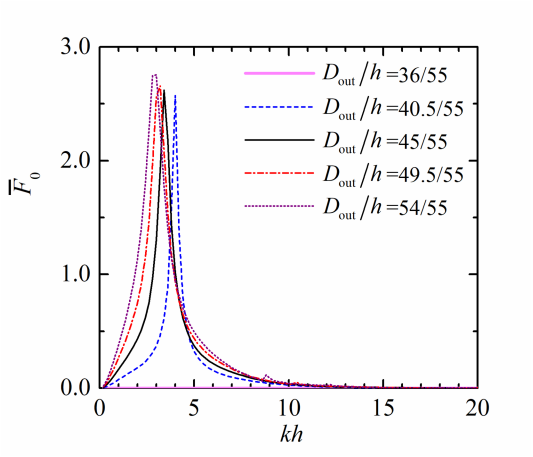

Figure 15: Effect of the outer hull width of a square hollow platform on wave excitation volume flux, $\bar{F}_0$.

spectively. The excellent agreement of the present results with the numerical ones gives confidence of the present semi-analytical model in solving water wave scattering problem of a truncated cylinder with a moonpool of arbitrary cross-section, such as the cylinders with a cosine-function-shaped cross section and an elliptic cross section. Nevertheless, when the shape of the cross section is rather different from a circular shape, the present model may not be able to solve the wave diffraction accurately for some specified wave frequencies.

5. Conclusions

A semi–analytical model is developed based on the linear potential flow theory to solve wave diffraction problem of a truncated cylinder with a moonpool of an arbitrary cross-section. The radius function associated terms are expressed as a Fourier series and an eigenfunction matching method is employed to determine the unknown coefficients in the velocity potentials.

The proposed semi–analytical model can be used to run benchmark tests and help validate numerical models. The results obtained by using WAMIT are found in remarkable agreement with the analytical results.

The semi-analytical model is adopted to examine the wave diffraction problems of an elliptic platform with different eccentricities and a square platform with different outer hull widths. For the elliptic platform with a fixed cross section area, the wave volume flux and also the wave frequencies where the sharp changes of the frequency response of the heave excitation force happen are found to be insensitive to the change of eccentricities. For a square platform with the area of cross-section fixed, the larger the moonpool, the smaller wave frequencies where the main sharp change of the frequency response of wave excitation forces/moments occurs. The peak of the frequency response of the wave excitation volume flux can be enlarged in terms of both bandwidth and height by using a larger moonpool.

Our attention is restricted to the wave diffraction problem of a stationary truncated cylinder with a moonpool. When the cylinder is free-floating, and/or the moonpool works as an OWC chamber to capture wave power, for which air pressure oscillation inside the chamber (i.e., above the moonpool) exists, the wave radiation problem appears as a result of the cylinder's oscillation and/or the internal air pressure oscillation. The semi-analytical model proposed in this paper can be easily extended to solve the wave radiation problem (e.g., see Zheng et al., 2019a, 2020a).

The present model is developed based on the usual assumptions of linearized wave-body interactions; hence the nonlinear and viscous effects are neglected. In contrast, these effects should be considered in order to achieve more realistic predictions of the wave excitation/moment acting on the cylinder and the wave motion inside the moonpool, especially for extreme and/or resonant wave conditions.

Acknowledgements

The research was supported by the Open Research Fund Program of State Key Laboratory of Coastal and Offshore Engineering, Dalian University of Technology (LP1928) and the Open Research Fund Program of State Key Laboratory

of Ocean Engineering, Shanghai Jiao Tong University (Grant No. 1916).

Appendix A. Integral equations of the diffraction problem

By multiplying Eqs. (17) and (18) with $\cos[\beta_\zeta(z+h)]\mathrm{e}^{-\mathrm{i}\tau\theta}/(h-d)$ and integrating over the range $0<\theta<2\pi$, $-h<z<-d$, multiplying Eqs. (19) and (20) with $Z_\zeta(z)\mathrm{e}^{-\mathrm{i}\tau\theta}/h$ and integrating over the range $0<\theta<2\pi$, $-h<z<0$, we get for any integer ζ and τ, four algebraic systems for the unknown coefficients $A_{m,l}$, $B_{m,l}$, $C_{m,l}$ and $D_{m,l}$:

$$\begin{aligned}&-\sum_{m=-\infty}^{\infty}\Lambda^{1,A}_{m,\tau,\zeta}A_{m,\zeta}-\sum_{m=-\infty}^{\infty}\Lambda^{1,B}_{m,\tau,\zeta}B_{m,\zeta}+\sum_{m=-\infty}^{\infty}\sum_{l=0}^{\infty}C_{m,l}L_{l,\zeta}\Lambda^{1,C}_{m,\tau,l}\\&=\frac{\mathrm{i}gA}{\omega}L_{0,\zeta}\sum_{m=-\infty}^{\infty}\mathrm{i}^m\mathrm{e}^{-\mathrm{i}m\beta}f^{J,in}_{m,0,\tau-m},\end{aligned}\tag{A.1}$$

$$\begin{aligned}&-\sum_{m=-\infty}^{\infty}\Lambda^{2,A}_{m,\tau,\zeta}A_{m,\zeta}-\sum_{m=-\infty}^{\infty}\Lambda^{2,B}_{m,\tau,\zeta}B_{m,\zeta}+\sum_{m=-\infty}^{\infty}\sum_{l=0}^{\infty}D_{m,l}L_{l,\zeta}\Lambda^{2,D}_{m,\tau,l}\\&=\frac{\mathrm{i}gA}{\omega}L_{0,\zeta}\sum_{m=-\infty}^{\infty}\mathrm{i}^m\mathrm{e}^{-\mathrm{i}m\beta}f^{J,out}_{m,0,\tau-m},\end{aligned}\tag{A.2}$$

$$\begin{aligned}&-\frac{h-d}{h}Z_\zeta(0)\sum_{m=-\infty}^{\infty}\sum_{l=0}^{\infty}\left(A_{m,l}\Lambda^{3,A}_{m,\tau,l}+B_{m,l}\Lambda^{3,B}_{m,\tau,l}\right)L_{\zeta,l}\\&\qquad+\sum_{m=-\infty}^{\infty}C_{m,\zeta}\Lambda^{3,C}_{m,\tau,\zeta}=\frac{\mathrm{i}gA}{\omega}\frac{\delta_{0,\zeta}}{Z_0(0)}\sum_{m=-\infty}^{\infty}\mathrm{i}^m\mathrm{e}^{-\mathrm{i}m\beta}f^{J',in}_{m,0,\tau-m},\end{aligned}\tag{A.3}$$

and

$$\begin{aligned}&-\frac{h-d}{h}Z_\zeta(0)\sum_{m=-\infty}^{\infty}\sum_{l=0}^{\infty}\left(A_{m,l}\Lambda^{4,A}_{m,\tau,l}+B_{m,l}\Lambda^{4,B}_{m,\tau,l}\right)L_{\zeta,l}\\&\qquad+\sum_{m=-\infty}^{\infty}D_{m,\zeta}\Lambda^{4,D}_{m,\tau,\zeta}=\frac{\mathrm{i}gA}{\omega}\frac{\delta_{0,\zeta}}{Z_0(0)}\sum_{m=-\infty}^{\infty}\mathrm{i}^m\mathrm{e}^{-\mathrm{i}m\beta}f^{J',out}_{m,0,\tau-m},\end{aligned}\tag{A.4}$$

where

$$\begin{aligned}L_{l,\zeta}&=\frac{1}{h-d}\int_{-h}^{-d}\frac{Z_l(z)\cos[\beta_\zeta(z+h)]}{Z_l(0)}\mathrm{d}z\\&=\begin{cases}\frac{(-1)^\zeta(h-d)k_0\sinh[k_0(h-d)]}{[(h-d)^2k_0^2+\zeta^2\pi^2]\cosh(k_0h)}, & l=0;\ \zeta=0,1,2,\cdots\\ \frac{(-1)^\zeta(h-d)k_l\sin[k_l(h-d)]}{[(h-d)^2k_l^2-\zeta^2\pi^2]\cos(k_lh)} & l=1,2,3,\cdots;\ \zeta=0,1,2,\cdots\end{cases},\end{aligned}\tag{A.5}$$

$$\Lambda^{1,A}_{m,\tau,\zeta} = \begin{cases} f^{RA,in}_{m,0,\tau-m}, & \zeta = 0 \\ \frac{1}{2}\tilde{f}^{I,in}_{m,\zeta,\tau-m}, & \zeta = 1,2,3,\cdots \end{cases}, \tag{A.6}$$

$$\Lambda^{1,B}_{m,\tau,\zeta} = \begin{cases} f^{RB,in}_{m,0,\tau-m}, & \zeta = 0 \\ \frac{1}{2}\tilde{f}^{K,in}_{m,\zeta,\tau-m}, & \zeta = 1,2,3,\cdots \end{cases}, \tag{A.7}$$

$$\Lambda^{1,C}_{m,\tau,\zeta} = \begin{cases} f^{J,in}_{m,0,\tau-m}, & \zeta = 0 \\ f^{I}_{m,\zeta,\tau-m}, & \zeta = 1,2,3,\cdots \end{cases}, \tag{A.8}$$

$$\Lambda^{2,A}_{m,\tau,\zeta} = \begin{cases} f^{RA,out}_{m,0,\tau-m}, & \zeta = 0 \\ \frac{1}{2}\tilde{f}^{I,out}_{m,\zeta,\tau-m}, & \zeta = 1,2,3,\cdots \end{cases}, \tag{A.9}$$

$$\Lambda^{2,B}_{m,\tau,\zeta} = \begin{cases} f^{RB,out}_{m,0,\tau-m}, & \zeta = 0 \\ \frac{1}{2}\tilde{f}^{K,out}_{m,\zeta,\tau-m}, & \zeta = 1,2,3,\cdots \end{cases}, \tag{A.10}$$

$$\Lambda^{2,D}_{m,\tau,l} = \begin{cases} f^{H}_{m,0,\tau-m}, & l = 0 \\ f^{K}_{m,l,\tau-m}, & l = 1,2,3,\cdots \end{cases}, \tag{A.11}$$

$$\Lambda^{3,A}_{m,\tau,l} = \begin{cases} \tilde{f}^{RA,in}_{m,0,\tau-m}, & l = 0 \\ \tilde{f}^{I',in}_{m,l,\tau-m}, & l = 1,2,3,\cdots \end{cases}, \tag{A.12}$$

$$\Lambda^{3,B}_{m,\tau,l} = \begin{cases} \tilde{f}^{RB,in}_{m,0,\tau-m}, & l = 0 \\ \tilde{f}^{K',in}_{m,l,\tau-m}, & l = 1,2,3,\cdots \end{cases}, \tag{A.13}$$

$$\Lambda^{3,C}_{m,\tau,\zeta} = \begin{cases} f^{J',in}_{m,0,\tau-m}/Z_0(0), & \zeta = 0 \\ f^{I'}_{m,\zeta,\tau-m}/Z_\zeta(0), & \zeta = 1,2,3,\cdots \end{cases}, \tag{A.14}$$

$$\Lambda^{4,A}_{m,\tau,l} = \begin{cases} \tilde{f}^{RA,out}_{m,0,\tau-m}, & l = 0 \\ \tilde{f}^{I',out}_{m,l,\tau-m}, & l = 1,2,3,\cdots \end{cases}, \tag{A.15}$$

$$\Lambda^{4,B}_{m,\tau,l} = \begin{cases} \tilde{f}^{RB,out}_{m,0,\tau-m}, & l = 0 \\ \tilde{f}^{K',out}_{m,l,\tau-m}, & l = 1,2,3,\cdots \end{cases}, \tag{A.16}$$

$$\Lambda^{4,D}_{m,\tau,\zeta} = \begin{cases} f^{H'}_{m,0,\tau-m}/Z_0(0), & \zeta = 0 \\ f^{K'}_{m,\zeta,\tau-m}/Z_\zeta(0), & \zeta = 1,2,3,\cdots \end{cases}, \tag{A.17}$$

in which the right-hand side terms of Eqs. (A.7)-(A.17) are the Fourier coefficients derived from the θ-dependent functions that are associated with r_{in} and r_{out}, and the detailed calculation and derivation process are given in Appendix B. The infinite series are truncated by choosing $m = -M, \cdots, M$ and $l = 0, 1, \cdots, L$. In the present studies, $M = 12$ and $L = 8$ are taken to obtain converged results.

Appendix B. Expressions of the Fourier coefficients derived from the θ dependent functions

The θ dependent functions may be written as a series of Fourier coefficients

$$J_m(k_0 r)\big|_{S_\chi=0} = \sum_{q=-\infty}^{\infty} f^{J,\chi}_{m,0,q} \mathrm{e}^{\mathrm{i}q\theta}, \tag{B.1}$$

$$\left(r^2 k_0 J'_m(k_0 r) + \mathrm{i}m J_m(k_0 r)\frac{\partial S_\chi}{\partial \theta}\right)\Big|_{S_\chi=0} = \sum_{q=-\infty}^{\infty} f^{J',\chi}_{m,0,q} \mathrm{e}^{\mathrm{i}q\theta}, \tag{B.2}$$

$$H_m(k_0 r)\big|_{S_{out}=0} = \sum_{q=-\infty}^{\infty} f^{H}_{m,0,q} \mathrm{e}^{\mathrm{i}q\theta}, \tag{B.3}$$

$$\left(r^2 k_0 H'_m(k_0 r) + \mathrm{i}m H_m(k_0 r)\frac{\partial S_{out}}{\partial \theta}\right)\Big|_{S_{out}=0} = \sum_{q=-\infty}^{\infty} f^{H'}_{m,0,q} \mathrm{e}^{\mathrm{i}q\theta}, \tag{B.4}$$

$$K_m(k_l r)\big|_{S_{out}=0} = \sum_{q=-\infty}^{\infty} f^{K}_{m,l,q} \mathrm{e}^{\mathrm{i}q\theta}, \tag{B.5}$$

$$\left(r^2 k_l K'_m(k_l r) + \mathrm{i}m K_m(k_l r)\frac{\partial S_{out}}{\partial \theta}\right)\Big|_{S_{out}=0} = \sum_{q=-\infty}^{\infty} f^{K'}_{m,l,q} \mathrm{e}^{\mathrm{i}q\theta}, \tag{B.6}$$

$$I_m(k_l r)\big|_{S_{in}=0} = \sum_{q=-\infty}^{\infty} f_{m,l,q}^{I} \mathrm{e}^{\mathrm{i}q\theta}, \tag{B.7}$$

$$\left(r^2 k_l I_m'(k_l r) + \mathrm{i}m I_m(k_l r)\frac{\partial S_{in}}{\partial \theta}\right)\Big|_{S_{in}=0} = \sum_{q=-\infty}^{\infty} f_{m,l,q}^{I'} \mathrm{e}^{\mathrm{i}q\theta}, \tag{B.8}$$

$$I_m(\beta_l r)\big|_{S_\chi=0} = \sum_{q=-\infty}^{\infty} \tilde{f}_{m,l,q}^{I,\chi} \mathrm{e}^{\mathrm{i}q\theta}, \tag{B.9}$$

$$\left(r^2 \beta_l I_m'(\beta_l r) + \mathrm{i}m I_m(\beta_l r)\frac{\partial S_\chi}{\partial \theta}\right)\Big|_{S_\chi=0} = \sum_{q=-\infty}^{\infty} \tilde{f}_{m,l,q}^{I',\chi} \mathrm{e}^{\mathrm{i}q\theta}, \tag{B.10}$$

$$K_m(\beta_l r)\big|_{S_\chi=0} = \sum_{q=-\infty}^{\infty} \tilde{f}_{m,l,q}^{K,\chi} \mathrm{e}^{\mathrm{i}q\theta}, \tag{B.11}$$

$$\left(r^2 \beta_l K_m'(\beta_l r) + \mathrm{i}m K_m(\beta_l r)\frac{\partial S_\chi}{\partial \theta}\right)\Big|_{S_\chi=0} = \sum_{q=-\infty}^{\infty} \tilde{f}_{m,l,q}^{K',\chi} \mathrm{e}^{\mathrm{i}q\theta}, \tag{B.12}$$

$$r^{|m|}\big|_{S_\chi=0} = \sum_{q=-\infty}^{\infty} f_{m,0,q}^{RA,\chi} \mathrm{e}^{\mathrm{i}q\theta}, \tag{B.13}$$

$$\left(|m| r^{|m|+1} + \mathrm{i}m r^{|m|}\frac{\partial S_\chi}{\partial \theta}\right)\Big|_{S_\chi=0} = \sum_{q=-\infty}^{\infty} \tilde{f}_{m,0,q}^{RA,\chi} \mathrm{e}^{\mathrm{i}q\theta}, \tag{B.14}$$

$$\sum_{q=-\infty}^{\infty} f_{m,0,q}^{RB,\chi} \mathrm{e}^{\mathrm{i}q\theta} = \begin{cases} \ln(r)|_{S_\chi=0}, & m=0 \\ r^{-|m|}|_{S_\chi=0}, & m\neq 0 \end{cases}, \tag{B.15}$$

$$\sum_{q=-\infty}^{\infty} \tilde{f}_{m,0,q}^{RB,\chi} \mathrm{e}^{\mathrm{i}q\theta} = \begin{cases} \left(r + \mathrm{i}m\ln(r)\frac{\partial S_\chi}{\partial \theta}\right)\big|_{S_\chi=0}, & m=0 \\ -|m| r^{1-|m|} + \mathrm{i}m r^{-|m|}\frac{\partial S_\chi}{\partial \theta}\big|_{S_\chi=0}, & m\neq 0 \end{cases}, \tag{B.16}$$

where χ represents *in* and *out*. The Fourier coefficients in the summation terms of the above equations can be evaluated from (Zheng et al., 2019c, 2020b)

$$U_{m,l,q} = \frac{1}{2\pi}\int_{-\pi}^{\pi} V_{m,l}(\theta)\mathrm{e}^{-\mathrm{i}q\theta}\mathrm{d}\theta \tag{B.17}$$

where $U_{m,l,q}$ represent the Fourier coefficients and $V_{m,l}(\theta)$ denotes the θ dependent items as given on the non-summation side of Eqs. (B.1)-(B.16).

References

Bozzi, S., Miquel, A.M., Scarpa, F., Antonini, A., Archetti, R., Passoni, G., Gruosso, G., 2013. Wave energy production in italian offshore: Preliminary design of a point absorber with tubular linear generator, in: 2013 International Conference on Clean Electrical Power (ICCEP), pp. 203–208.

Chen, X.B., Liu, H.X., Duan, W.Y., 2015. Semi-analytical solutions to wave diffraction of cylindrical structures with a moonpool with a restricted entrance. Journal of Engineering Mathematics 90, 51–66.

Dodd, J., 2015. Analysis: France aims to be expert in floating technology. URL: `https://www.windpowermonthly.com/article/1357312/analysis-france-aims-expert-floating-technolgy`.

Evans, D.V., Porter, R., 1995. Hydrodynamic characteristics of an oscillating water column device. Applied Ocean Research 17, 155–164.

Evans, D.V., Porter, R., 1997. Efficient calculation of hydrodynamic properties of OWC-type devices. Journal of Offshore Mechanics and Arctic Engineering 119, 210–218.

Garrett, C.J.R., 1970. Bottomless harbours. Journal of Fluid Mechanics 43, 433–449.

Guo, X., Lu, H., Yang, J., Peng, T., 2017. Resonant water motions within a recessing type moonpool in a drilling vessel. Ocean Engineering 129, 228 – 239.

Hammargren, E., Törnblom, J., 2012. Effect of the Moonpool on the Total Resistance of a Drillship. Ph.D. thesis. Chalmers University of Technology. Gothenburg, Sweden.

Laughlin, R.B., 2010. Oceaneering international web site - 2010, heavy weather deployment. URL: `http://large.stanford.edu/publications/coal/references/ocean/rovs/heavy/`.

Liu, H., Chen, H., Zhang, L., Zhang, W., Liu, M., 2017. Quadratic dissipation effect on the moonpool resonance. China Ocean Engineering 31, 665–673.

Liu, Y., 2019. HAMS: A frequency-domain preprocessor for wave-structure interactions—theory, development, and application. Journal of Marine Science and Engineering 7, 81.

Mavrakos, S.A., 1985. Wave loads on a stationary floating bottomless cylindrical body with finite wall thickness. Applied Ocean Research 7, 213–224.

Mavrakos, S.A., 1988. Hydrodynamic coefficients for a thick-walled bottomless cylindrical body floating in water of finite depth. Ocean Engineering 15, 213 – 229.

Mavrakos, S.A., Konispoliatis, D.N., 2012. Hydrodynamics of a free floating vertical axisymmetric oscillating water column device. Journal of Applied Mathematics 2012, 1 – 27.

Miloh, T., 1983. Hydrodynamical loads on a floating solar pond, in: International Workshop on Ship and Platform Motion, pp. 110–131.

Miquel, A., Lamberti, A., Antonini, A., Archetti, R., 2020. The moonwec, a new technology for wave energy conversion in the mediterranean sea. Ocean Engineering 217, 107958.

Miquel, A.M., Antonini, A., Archetti, R., Bozzi, S., Lamberti, A., 2017. Nonlinear modelling of a heaving point absorber: The surge effect. International Journal of Marine Energy 19, 95 – 109.

Molin, B., 2001. On the piston and sloshing modes in moonpools. Journal of Fluid Mechanics 430, 27–50.

Molin, B., Zhang, X., Huang, H., Remy, F., 2018. On natural modes in moonpools and gaps in finite depth. Journal of Fluid Mechanics 840, 530–554.

Wei, Y., Yang, J., Chen, G., Hu, Z., 2011. The research of moonpool size effect on the hydrodynamic performance of fdpso, in: Proceedings of the

ASME 2011 30th International Conference on Ocean, Offshore and Arctic Engineering, Rotterdam, The Netherlands. pp. 459–467.

Zheng, S., Antonini, A., Zhang, Y., Greaves, D., Miles, J., Iglesias, G., 2019a. Wave power extraction from multiple oscillating water columns along a straight coast. Journal of Fluid Mechanics 878, 445–480.

Zheng, S., Zhang, Y., 2017. Analysis for wave power capture capacity of two interconnected floats in regular waves. Journal of Fluids and Structures 75, 158 – 173.

Zheng, S., Zhang, Y., Iglesias, G., 2019b. Coast/breakwater-integrated OWC: A theoretical model. Marine Structures 66, 121–135.

Zheng, S., Zhang, Y., Iglesias, G., 2020a. Concept and performance of a novel wave energy converter: Variable Aperture Point-Absorber (VAPA). Renewable Energy 153, 681 – 700.

Zheng, S., Zhang, Y., Liu, J., Iglesias, G., 2020b. Wave diffraction from multiple truncated cylinders of arbitrary cross sections. Applied Mathematical Modelling 77, 1425 – 1445.

Zheng, S., Zhang, Y., Liu, Y., Iglesias, G., 2019c. Wave radiation from multiple cylinders of arbitrary cross sections. Ocean Engineering 184, 11–22.

Zhou, H., Zhang, H., 2013. Radiation and diffraction analysis of a cylindrical body with a moon pool. Journal of Hydrodynamics, Ser. B 25, 196 – 204.

Zhu, S., Mitchell, L., 2009. Diffraction of ocean waves around a hollow cylindrical shell structure. Wave Motion 46, 78 – 88.